Numerical Model of the Mars Electrostatic Precipitator

Jerry J. Wang, Joel D. Malissa, James R. Philips III, Michael R. Johansen, Carlos I. Calle
NASA Kennedy Space Center, KSC, FL, USA

Abstract
NASA's future human exploration missions will require chemical processing plants to convert local resources into consumables to support astronaut activities [1]. The thin and mostly carbon dioxide atmosphere of Mars is estimated to have 1 – 10 particles/cm^3 with diameters of 1 – 10 μm and up to 1000 particles/cm^3 during storms [2]. The dust in the Martian atmosphere can foul chemical reactors and pose a risk to life support systems. Electrostatic precipitation (ESP) removes dust particles from the Martian atmosphere. The Electrostatics and Surface Physics Laboratory at NASA's Kennedy Space Center has developed a COMSOL Multiphysics® model of an ESP for dust filtration on Mars. The fundamental principles of an ESP can be simulated by four physics modules: plasma, AC/DC electromagnetics, computational fluid dynamics (CFD), and particle tracing. In the ESP model presented here, the plasma module was solved to estimate particle charge. The AC/DC and CFD module were solved for the electrostatic force and fluid force. The particle-tracing module was solved for particle collection efficiency.

Introduction

NASA's future human missions will include the use of in-situ resource utilization (ISRU) technology to convert on-site resources to consumables. One of these resources on Mars is the thin and mostly carbon dioxide atmosphere. The carbon dioxide-rich atmosphere, when combined with hydrogen gas, can be converted to methane for rocket propellant and oxygen for life support through the Sabatier reaction. However, the Mars atmosphere contains fine particles with diameters ranging from 1 μm to 10 μm at a density of 1 to 10 particles per cm^3 on average and 100 to 1000 particles per cm^3 during a dust storm [3]. These dust particles must be removed from the chemical conversion process to produce high consumables and to prevent the processing plant from deteriorating. The ESP is one option to clear dust particles from low-pressure Mars ISRU plant intakes.

The ESP utilizes corona discharge to perform dust collection. The corona discharge forms around the high voltage wire and ions with the same polarity as the wire are repelled toward the grounded cylinder. These ions attach to dust particles flowing through the cylinder due to the distortion of the electric field [4]. Charged dust particles experience a force in the electric field that carries them to the grounded cylinder. Earth based ESP have a collection efficiency greater than 99%; however, Mars' atmosphere is approximately 4.75 Torr (less than 1% of Earth's atmosphere) and approaches the Paschen minimum for many useful geometries. This constraint limits the amount of voltage applied in the Martian ESP to obtain the high collection efficiency. Previous work developed a testbed to demonstrate the feasibility of an ESP in Martian conditions and the COMSOL Multiphysics® model presented in this paper numerically estimates the collection efficiency [5].

Model description and equations
The fundamental principles of an ESP is split into four COMSOL physics modules: DC plasma, electrostatics, laminar flow, and particle tracing. The plasma module solves first followed by all others in parallel.

DC plasma

The Mars ESP plasma model is similar to the "Atmospheric Pressure Corona Discharge in Air" model from the plasma module library. The plasma model is a one-dimensional geometry and the corona discharge is set as diffuse and uniform in the radial direction. The high voltage electrode diameter is 125 μm and the grounded cylinder's inner diameter is 7.1cm. The simulation solves for the steady state regime with corona discharge sustained between 4.75 Torr and 7 Torr with CO_2 gas.

The electron and ion continuity equation, the momentum equation, the drift diffusion approximation, and the Poisson's equation determine the electron and charged species [6]. The electron energy distribution function (EEDF) provides the relationship between mean electron energy and reduced electric field to minimize the computation time and decrease the model complexity [7].

For corona discharge, the Maxwellian shape function describes the EEDF since the ionization degree is high inside the corona discharge region and inelastic reactions are dominate [7].

$$f(\epsilon) = \varphi^{-\frac{3}{2}}\beta_1 \exp(-\frac{\epsilon\beta_2}{\varphi})$$

$$\beta_1 = \Gamma\left(\frac{5}{2}\right)^{\frac{3}{2}}\Gamma\left(\frac{3}{2}\right)^{\frac{-5}{2}}$$

$$\beta_2 = \Gamma\left(\frac{5}{2}\right)\Gamma\left(\frac{3}{2g}\right)^{-1}$$

ϵ is the electron energy (eV), φ is the mean electron energy (eV), g is the power factor of 1 for Maxwellian distribution, and Γ is the incomplete Gamma function. Online plasma databases provide the collision data to calculate the EEDF [8].

The following equation determines the non-electron species density

$$\rho\frac{\partial}{\partial t}(\omega_k) + \rho(\boldsymbol{u}\cdot\nabla)\omega_k = \nabla\cdot\boldsymbol{j_k} + R_k$$

Where ρ is the species density, ω_k is the mass fraction of k_{th} species, R_k is the rate expression for species k, $\boldsymbol{u}$ is the mass averaged fluid velocity, and $\boldsymbol{j_k}$ is the diffusive flux vector.

The Mars ESP uses positive polarity corona discharge to ionize the carbon dioxide gas. Previous experimental work showed the positive polarity corona discharge in Martian atmosphere is more stable than the negative polarity. However, higher voltage potential is required to initiate the discharge; this is likely due to the faster electron mobility when compared with ion mobility [5].

Laminar Flow

The Navier-Stokes equation solves the velocity components and pressure gradients in the model domain.

$$-\eta\nabla^2\boldsymbol{u} + \rho(\boldsymbol{u}\cdot\nabla)\boldsymbol{u} + \nabla p = \boldsymbol{F}$$

$$\nabla\cdot\boldsymbol{u} = 0$$

The first equation is from the balance of momentum based on Newton's second law and the second is the continuity equation. Where η is the dynamic viscosity, $\boldsymbol{u}$ is the velocity components, ρ is the density, p is the pressure, and $\boldsymbol{F}$ is the force field.

The no slip condition is enforced on the wall boundaries, and the carbon dioxide fluid properties are provided from the basic materials properties library. The simulation temperature is set at room temperature, and the pressure inside the simulation domain is set at 4.75 Torr to resemble the Martian atmosphere. Fully developed flow with volumetric flow as the input is set as the inlet boundary condition. The flow rate is in the standard notation thus a conversion through combined gas law is required to convert from standard centimeter cube per min to cubic meter per second at the relevant condition.

$$\frac{P_1\dot{V}_1}{T_1} = \frac{P_2\dot{V}_2}{T_2}$$

Martian atmosphere pressure is set at the outlet boundary condition.

Electrostatics

The electrostatic module in COMSOL Multiphysics ® solves the static electric field by the combination of the definition of electric potential, the constitutive relationship equation, and the Gaussian law to yield the Poisson's equation form [6].

$$\boldsymbol{E} = -\nabla V$$

$$\boldsymbol{D} = \epsilon_0\boldsymbol{E} + \boldsymbol{P}$$

$$\nabla\cdot\boldsymbol{D} = \rho$$

Where $\boldsymbol{E}$ is the electric field intensity, V is the electric potential, $\boldsymbol{D}$ is the displacement field, $\boldsymbol{P}$ is the electric polarization vector, and ρ is the electric charge density.

By substituting the electric potential definition into the constitutive relationship equation yields

$$\boldsymbol{D} = -\epsilon_0\nabla V + \boldsymbol{P}$$

By apply the new constitutive relationship back into the Gaussian law yields Poisson's equation accounting for the presence of dielectrics inside an electric field.

$$-\nabla\cdot(\epsilon_0\nabla V - \boldsymbol{P}) = \rho$$

The electric potential at the wire is at the highest potential without entering corona breakdown. Previous work recorded the value of corona breakdown voltage [2]. The ground potential is set for the inner wall and the material library provides the carbon dioxide dielectric constant.

Particle Tracing

The results from the previous modules provide the particle charge, electric field strength, and the aerodynamic force for the particle-tracing module. The electrostatic force experienced by each particle is expressed as

$$\boldsymbol{F} = q\boldsymbol{E}$$

Where q is the particle charge and $\boldsymbol{E}$ is the electric field vector. The particle charge is based on the positive ion density from the plasma model. The positive ion density represents the number of available ions that can attach to the surface of a particle. The field charging equation (Pauthenier charging mechanism) estimates the particle charge [4].

$$q = q_{max}\left[\frac{1}{1+\frac{\tau}{t}}\right]$$

$$q_{max} = 4\pi\varepsilon_0 r^2 p|\boldsymbol{E}|$$

$$\tau = \frac{4\varepsilon_0}{N_0 e b}$$

$$p = \frac{3\varepsilon_r}{\varepsilon_r + 2}$$

Where q_{max} is the maximum charge, r is particle radius, ε_0 is the vacuum permittivity, ε_r is the relative permittivity, τ is the time for the particle to reach half charge, N_0 is the ion density, e is the electron charge, and b is the ion mobility.

The Coulomb force between particle-particle interactions is expressed in the model as

$$\boldsymbol{F} = \frac{e^2}{4\pi\varepsilon_0}\sum_{j=1}^{N} ZZ_j \frac{r - r_j}{\left|r - r_j\right|^3}$$

Where Z is the charge number of the main particle, Z_j is the charge number on the j_{th} particle, r is the position of the main particle, and r_j is the position of the j_{th} particle [6].

The Stokes drag model with the Cunningham correction factor provides the aerodynamic force calculation for submicron particles.

Experimental set-up

Previous work developed the Mars ESP testbed to characterize the dust collection efficiency. The testbed consists of a stainless steel tube that is 1 m long and has an inner diameter of 7.1 cm. A 125 µm diameter stainless steel wire suspends at the center of the tube as the high voltage electrode. Combination of mass flow controllers, upstream and downstream pressure controllers maintain a constant pressure at flow range from 0 to 20,000 SCCM inside the precipitator, as shown in **Error! Reference source not found.**.

The fluidized dust bed injects the Mars dust simulant into the test section, as shown in **Error! Reference source not found.**. Two fine particle analyzers (FPA) sample the upstream and downstream dust flow injected from the fluidized bed. The flow velocity measured downstream of each FPA determines the FPA inlet efficiency to extrapolate the actual dust density from the measured FPA value. The laser side scatter method (LSSM) validated the dust density extrapolation; the LSSM is setup downstream of the test section where the flow passes into a vacuum chamber with transparent view ports as shown in Figure 3.

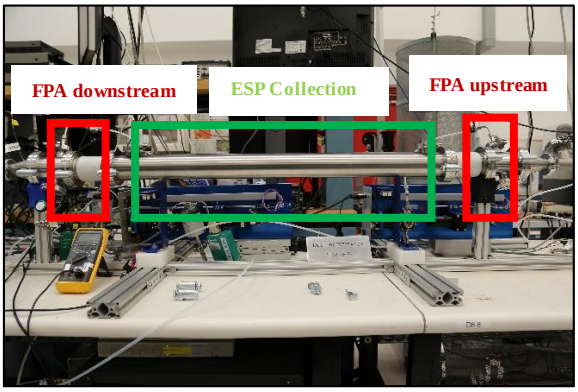

Figure 1: ESP testbed collection region

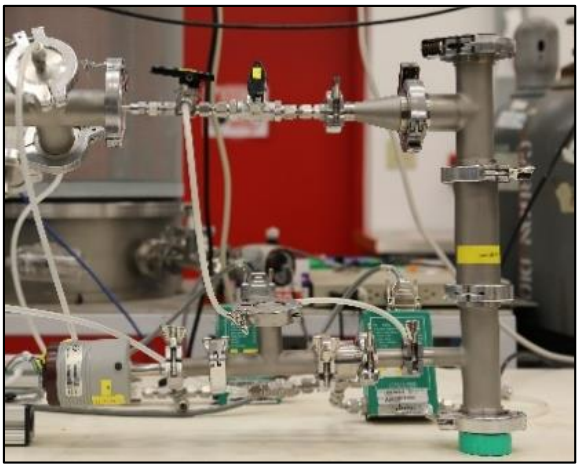

Figure 2: Fluidized dust bed to inject dust particles into the ESP

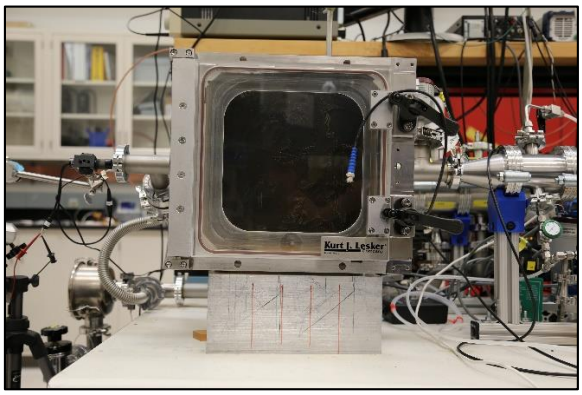

Figure 3: ESP testbed downstream chamber for laser scattering

Tests were performed with pure carbon dioxide gas; previous work shows that carbon dioxide is a qualitatively similar substitute for Mars gas simulant (shown below in Figure 4) [2].

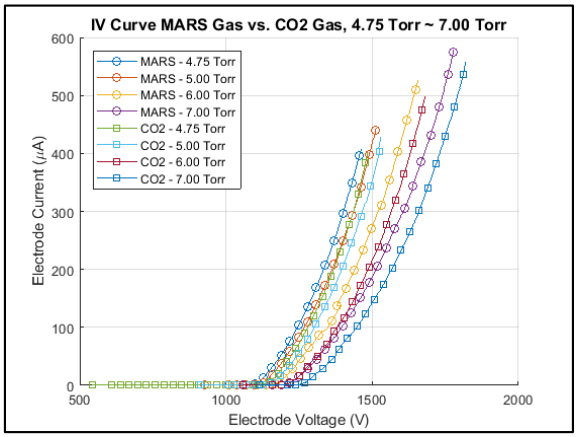

Figure 4: Corona current vs. voltage for carbon dioxide and Mars gas simulant [2]

Results

The first parameters in the model that must be determined are the electron and ion density distribution inside the precipitator. Figure 5 to Figure 10 below shows the density distribution for a positive 1350 V corona in a 7.1 cm precipitator. The electron number density close to the positive electrode where the corona region takes place is approximately $10^{13}\ m^{-3}$ and falls off quickly away from the wire. The negative ions, O^- and O_2^-, are both approximately $10^9 - 10^{10}$ and can be neglected when compared to that of electrons.

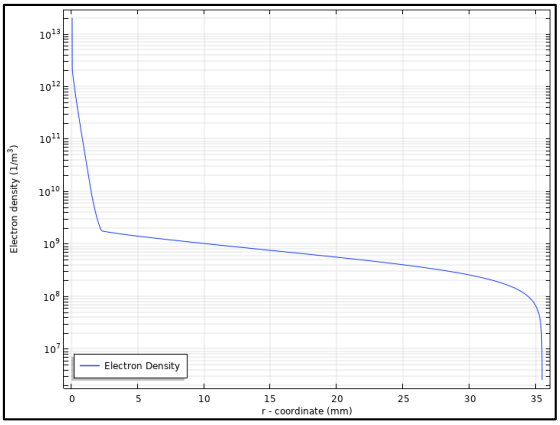

Figure 5: Electron density distribution across the precipitator 1-D symmetric setup

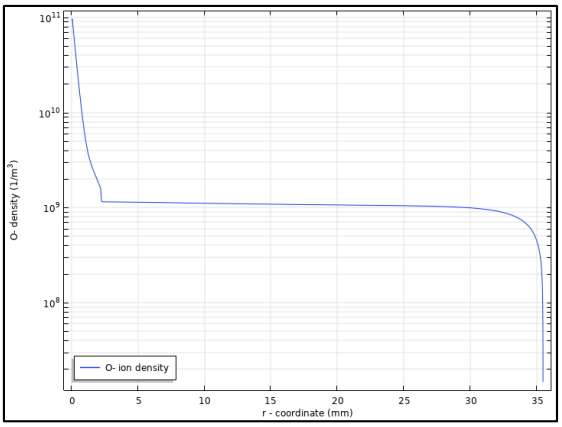

Figure 6: O- density distribution across the precipitator 1-D symmetric setup

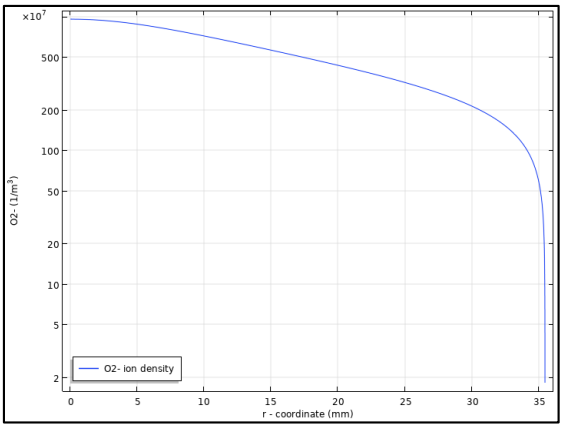

Figure 7: O2- density distribution across the precipitator 1-D symmetric setup

The density distribution of positive ions are on the order of $10^{13}$for CO_2 in most regions of the ESP and $10^{10} - 10^{11}$ for O^+ and O_2^+. The positive ions dominate the overall charge distribution since the

positive ions density is two orders of magnitudes larger than the negative density. This is as expected for a positive corona and the dust particle entering into the precipitator should acquire a positive charge. Note that the O^- density shows a uniform density distribution across the radial direction instead of peaking near the wire and drop off toward the collection electrode, this result is unexpected. However, since the order of magnitude of O^- density is negligible compared to that of CO_2^+ ions, the overall result of the model is unaffected. The computed distributions of O_2^+ and CO_2^+ are higher in the corona region where ions are generated and decrease as ions migrate away towards ground in the positive electric field.

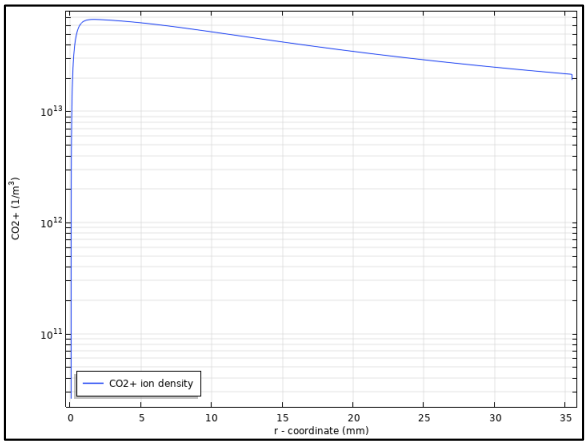

Figure 8: CO2+ density distribution across the precipitator 1-D symmetric setup

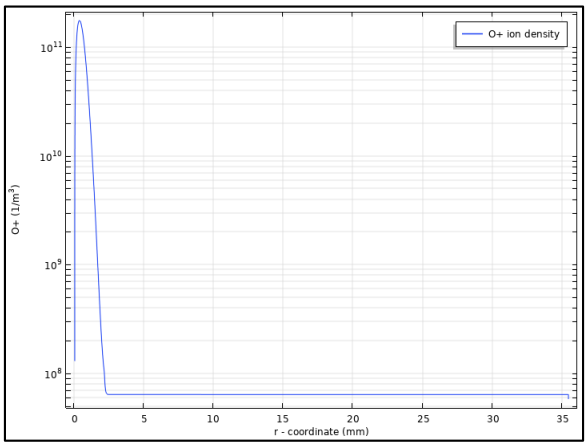

Figure 9: O+ density distribution across the precipitator 1-D symmetric setup

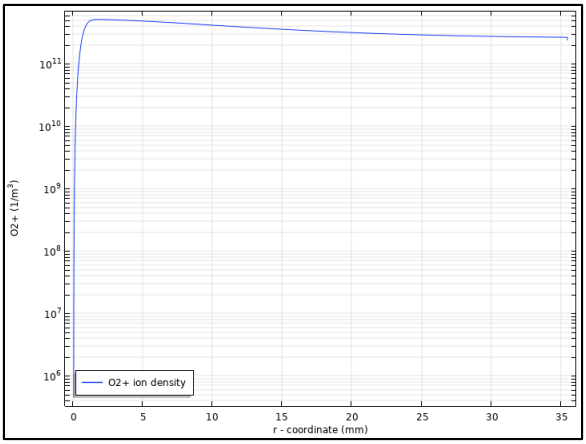

Figure 10: O2+ density distribution across the precipitator 1-D symmetric setup

It is possible to compare the simulation and theoretical corona current to electrode voltage relationship. The knowledge of this current-voltage (I-V) relationship provides insight into the charge acquired by a dust particle inside the ESP.

Figure 11 shows the theoretical and experimental IV curve for the 7.1 cm diameter precipitator at 4.75 Torr. For a given pressure, the potential to the high voltage electrode is slowly increased from 0 V to 1400 V in steps of 50 V. Initially, the corona remains at zero while the voltage increases. This is the recombination stage where the electrons do not have enough energy from the electric field and recombines with the ions. As voltage increases to an onset value, the strengthened electric field provides the electrons enough energy to maintain the ionization and starting an electron avalanche. The current is the small electric current carried by the positive ions that migrate from the corona region toward the ground electrode wall. If the voltage is increased further, the corona current increases rapidly and the glow region expands until it become unstable.

The COMSOL-generated I-V curve qualitatively approximates the shape and magnitude of experimental results. The current values meet close to the start of corona instability. This is the region of interest since it provides the strongest electric field across the precipitator. The model predicted the onset of the corona voltage prematurely; this may be from the Maxwellian approximation's assumption that all particles have high ionization levels. Further refinement of the model and different EEDF approximation methods may provide a better fit to the experimental curve.

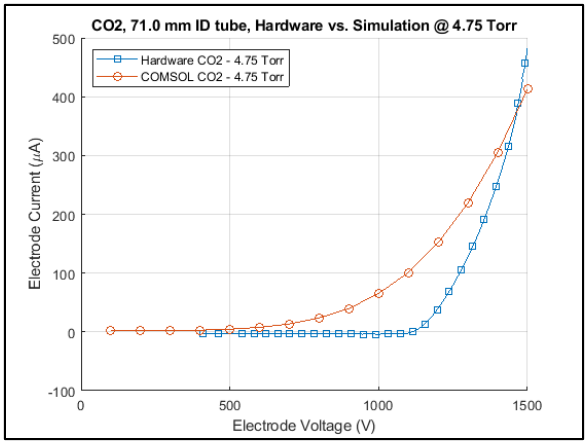

Figure 11: Experimental and simulated corona current vs. voltage results

Given the estimation of the charge on dust particles, predictions on the particle trajectory is determined to provide the optimal geometry for Mars ISRU intakes. Various particle diameters simulated at different flow rates are shown in Figure 12 to Figure 15. Simulated particles have diameters that match the average diameter of dust particles in the Martian atmosphere. An estimate for the expected charge of a dust particle in the low-pressure Martian atmosphere is $1\ \frac{fC}{\mu m}$ [9]. This estimate is one order of magnitude greater than the calculated charge from the COMSOL plasma module; therefore, the trajectory analysis overestimates the distance travelled. The trajectory simulation results are shown in the figures below.

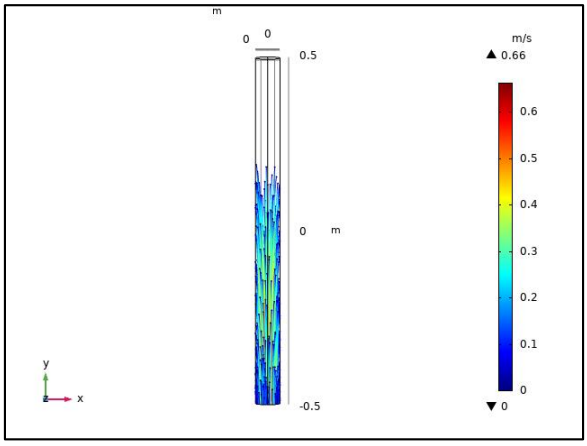

Figure 12: Particle tracing for 1 μm particles with $2.139 * 10^{-16}$ C at 500 SCCM and 4.75 Torr

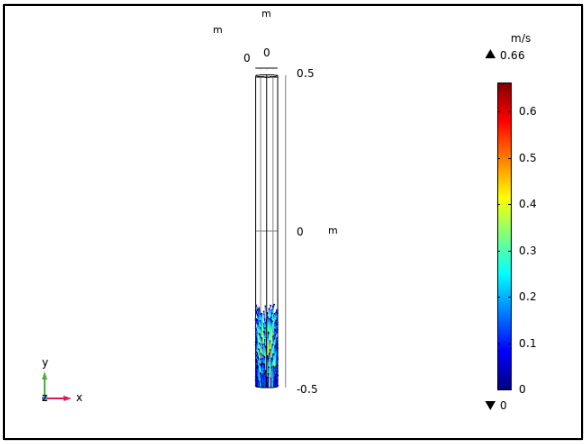

Figure 13: Particle tracing for 3 μm particles with $1.925 * 10^{-15}$ C at 500 SCCM and 4.75 Torr

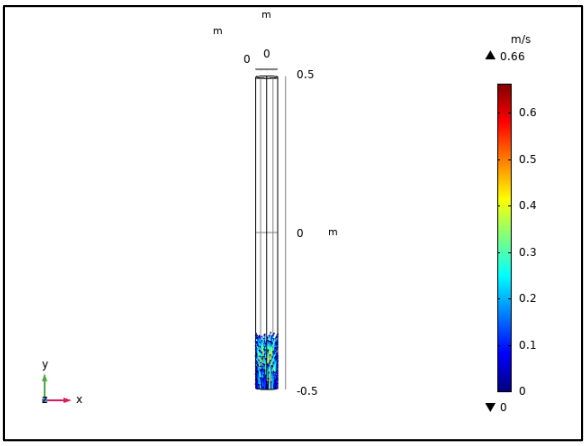

Figure 14: Particle tracing for 5 μm particles with $5.349 * 10^{-15}$ C at 500 SCCM and 4.75 Torr

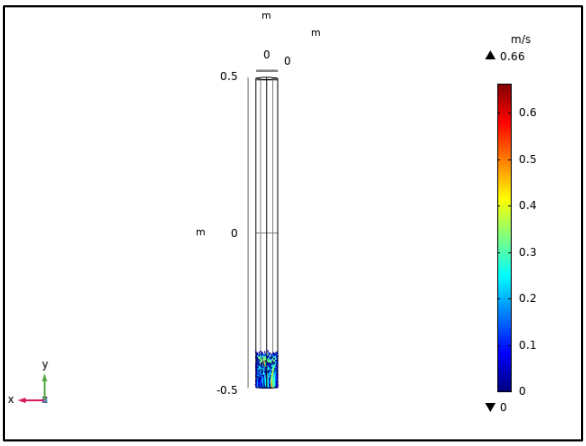

Figure 15: Particle tracing for 10 μm particles with $2.139 * 10^{-14}$ C at 500 SCCM and 4.75 Torr

As shown above, the required collection length increases as the particle size decreases from 10 μm to

1 μm. 1 μm particles follow the fluid streamlines further along the tube and their smaller size receives less charge for electrostatic precipitation.

The collection efficiency equation below provides the overall efficiency of an ESP. The theoretical efficiency takes account of the migration velocity and the electric field strength at the high voltage electrode and the ground electrode but does not account for particle-to-particle interaction, and gravity.

$$\eta_{theoretical} = 100 * (1 - e^{\frac{-A*w}{V_f}})$$

$$w = \frac{2 * \varepsilon_0 E_c E_p \left(\frac{d}{2}\right)}{\eta_{CO2}}$$

Where A is the collection area, w is the particle migration velocity, ε_0 is the permittivity of free space, E_c is the field strength at the wire, E_p is the field strength at the wall, d is the particle diameter, and η_{CO2} is the carbon dioxide dynamic viscosity.

The other efficiency equation is dependent on ratio of particle entering and existing the collection zone. This is the efficiency calculation for both the particle-tracing model and the ESP testbed.

$$\eta_c = \left(1 - \frac{\rho_s}{\rho_e}\right) * 100$$

Where ρ_s is the particle density leaving the collection zone and ρ_e is the particle density entering the collection zone from the inlet.

The table below lists the theoretical particle collection efficiencies, COMSOL results, fine particle analyzer measurements, and LSSM measurements.

Table 1: Analytical, numerical, and experimental collection efficiency results

Diameter (μm)	$\eta_{theoretical}$	η_{COMSOL}	η_{FPA}	η_{Laser}
1	77.8%	100.0%	99.6%	90.0%
3	98.8%	100.0%	99.5%	95.0%
5	99.9%	100.0%	99.7%	90.0%
10	100.0%	100.0%	99.0%	90.0%

The collection efficiencies for sizes ≥ 3 µm show over 90% particle collection efficiency. The LSSM measurement is reduced by error from dust re-entrenchment downstream of the collection zone [10].

Conclusion

The purpose of this model is to obtain a preliminary assessment of an optimized ESP geometry for Mars ISRU. The ISRU plant is designed to operate on a normal day of 1-10 particles/cm^3, and results from the simulation and the testbed show that the ESP can provide a minimum of 90% collection efficiency in the event of a Mars dust storm with up to 1000 particles/cm^3. By expanding the same geometry in parallel and stacking in a honeycomb style shown in Figure 16, the ESP can accommodate higher volumetric flows to support human missions on Mars.

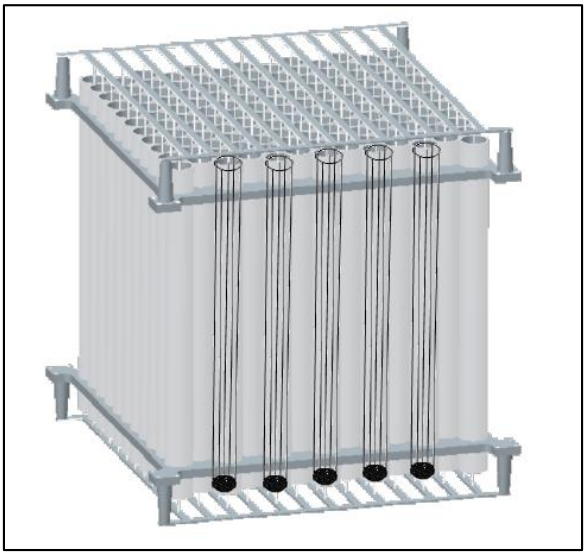

Figure 16: Preliminary assessment of an ESP geometry to support ISRU on Mars

Further refinement on the COMSOL plasma model is required to provide a better charge estimation. The plasma solution is highly dependent on the neutral and ion species used. The species were selected based on the strongest interaction inside the plasma region by a positive corona in the Martian atmosphere. The plasma model and EEDF approximation significantly reduced the computation time but sacrificed the accuracy to determine corona onset, future work will seek to improve the model by including additional species and ions as well as a different EEDF approximation.

The experimental setup effort is currently under review and the lessons learned will provide insight to the next generation of Mars ESP testbed. Two potential improvements are FPA sensors capable of detecting finer particles and design changes to mitigate dust re-entrenchment.

References

[1] G. Sanders, "Current NASA Plans for Mars In Situ Resource Utilization," NASA, 2018.

[2] M. Johansen, J. Phillips III, J. Wang, J. Mulligan, P. Mackey, J. Clements and C. Calle, "Electrical Characteristics of the Mars Electrostatic Precipitator," in *Electrostatics Joint Conference*, Boston, 2018.

[3] G. Landis, K. Herkenhoff, R. Greeley, S. Thompson, P. Whelley and a. t. M. A. S. Team, "Dust and Sane Deposition on the MER Solar Arrays as Viewed by the Microscopic Image," *Lunar Planet Sci.*, vol. 37, 1937.

[4] J. Cross, Electrostatics: Principles and Applications, London: IOP, 1987.

[5] J. Sidney, S. Thompson, N. Cox, M. Johansen, B. Williams, M. Hogue, M. Lowder, C. Calle, "Development of an Electrostatic Precipitator to Remove Martian Atmospheric Dust from ISRU Gas Intakes During Planetary Exploration Mission," in *IEEE Industry Applications Society Annual Meeting*, Orlando, 2011.

[6] D. J. Griffiths, Introduction to Electrodynamics, Boston: Pearson, 2003.

[7] A. Pahl, "Electron Energy Distribution Function," COMSOL, 2014. [Online]. Available: https://www.comsol.com/blogs/electron-energy-distribution-function.

[8] Itikawa, "Plasma Data Exchange Project," LXCat, 2010. [Online]. Available: www.lxcat.net.

[9] O. Melnik and M. Parrot, "Electrostatic Discharge in Martian Dust Storms," J. Geophy Res., 1998.

[10] B. Kemmerer, J. Lane, J. Wang, J. Phillips III, M. Johansen, C. Buhler and C. Calle, "Electrostatic Precipitator Dust Density Measurements in a Mars-Like Atmosphere," *submitted to Particulate Science and Technology, under review*, 2019.